

DISCOVERY OF MULTIPLY IMAGED GALAXIES BEHIND THE CLUSTER AND LENSED QUASAR SDSS J1004+4112¹

KEREN SHARON², ERAN O. OFEK², GRAHAM P. SMITH³, TOM J. BROADHURST², DAN MAOZ², CHRISTOPHER S. KOCHANEK⁴, MASAMUNE OGURI^{5,6}, YASUSHI SUTO⁵, NAOHISA INADA⁷, EMILIO E. FALCO⁸

Received 2005 June; accepted 2005 July

ABSTRACT

We have identified three multiply imaged galaxies in *Hubble Space Telescope* images of the redshift $z = 0.68$ cluster responsible for the large-separation quadruply lensed quasar, SDSS J1004+4112. Spectroscopic redshifts have been secured for two of these systems using the Keck I 10m telescope. The most distant lensed galaxy, at $z = 3.332$, forms at least four images, and an Einstein ring encompassing 3.1 times more area than the Einstein ring of the lensed QSO images at $z = 1.74$, due to the greater source distance. For a second multiply imaged galaxy, we identify Ly α emission at a redshift of $z = 2.74$. The cluster mass profile can be constrained from near the center of the brightest cluster galaxy, where we observe both a radial arc and the fifth image of the lensed quasar, to the Einstein radius of the highest redshift galaxy, ~ 110 kpc. Our preliminary modeling indicates that the mass approximates an elliptical body, with an average projected logarithmic gradient of $\simeq -0.5$. The system is potentially useful for a direct measurement of world models in a previously untested redshift range.

Subject headings: cosmology: observations – gravitational lensing – large-scale structure of universe – galaxies: clusters: individual (SDSS J1004+4112)

1. INTRODUCTION

The recent discovery of a quadruply lensed quasar, SDSS J1004+4112, with unusually large image separations (Inada et al. 2003, Oguri et al. 2004), has generated much interest. The quasar, at $z = 1.74$, is lensed by a galaxy cluster at $z = 0.68$ into four bright images on an Einstein ring of approximately 15'' in diameter. A faint fifth image is seen projected through the inner isophotes of the central brightest cluster galaxy (BCG; Inada et al. 2005). The QSO is known to vary in brightness. Assuming a nominal value for the Hubble parameter H_0 , it will be possible, for the first time, to model a cluster potential using complementary information on the value of the potential itself (from the measured time delays), rather than only constraints on the first derivative of the potential (i.e., multiple-image positions) and the second derivative of the potential (i.e., weak lensing). Finally, the partial Einstein ring, seen to pass through the lensed quasar images, is the most highly magnified quasar host galaxy known, permitting a unique probe of quasar hosts at $z = 1.7$ (Kochanek et al. 2005, in prep.).

Strong lensing is now being used to constrain in de-

tail the inner mass profile of galaxy clusters and for estimating the amount of sub-structure (e.g., Gavazzi et al. 2004, Kneib et al. 2003, Smith et al. 2005, Sand et al. 2004, Broadhurst et al. 2005a,b). A prediction of N-body simulations using the standard Λ -CDM cosmology (e.g., Navarro, Frenk, & White 1997, NFW; Moore et al. 1999) is that the logarithmic gradient of the density profile of the cluster should be shallower than that of an isothermal profile. In the case of A1689, where 30 background galaxies are found to be lensed into over 100 images (Broadhurst et al. 2005a), the profile does continuously flatten towards the center like an NFW profile, but with a surprisingly high concentration, $c_{vir} = 14 \pm 1.5$ (Broadhurst et al. 2005b), compared with the much more diffuse halos predicted for massive clusters, $c_{vir} \sim 4$ (e.g., Bullock et al. 2001). A1689 has the largest known Einstein ring, $\theta_E = 48''$ (for $z = 3$) and thus projection effects may be important (Oguri et al. 2005). A survey of more typical clusters is needed before drawing any general conclusions.

The Advanced Camera for Surveys (ACS) on the *Hubble Space Telescope* (HST) has an unparalleled advantage for lensing work, providing depth, spatial resolution and color information. Well resolved internal structure can be helpful in identifying counter-images of multiply imaged galaxies, particularly since distant star-forming galaxies often have complex and unique morphologies. A good lens model is required in order to take proper advantage of the resolved internal structure, as the parity and differential magnification of internal galaxy features varies between images of the same source, leading to confusion. Without guidance from a lens model, it is hard to recognize counter-images because they often fall in unexpected places due to deflections by substructure and cluster galaxies. The angular position, $\vec{\theta}_i$, of an image is given by the lens equation $\vec{\theta}_i = \vec{\beta}_s + (d_{ls}/d_s)\vec{\alpha}(\theta_i)$, where

¹ Based on observations made with the NASA/ESA *Hubble Space Telescope*, which is operated by AURA, Inc., under NASA contract NAS5-26555.

² School of Physics and Astronomy, Tel Aviv University, Tel-Aviv 69978, Israel

³ Department of Astronomy, California Institute of Technology, Mail Code 105-24, Pasadena, CA 91125

⁴ Department of Astronomy, Ohio State University, Columbus, OH 43210

⁵ Department of Physics, School of Science, University of Tokyo, Tokyo 113-0033, Japan

⁶ Department of Astrophysical Science, Princeton University, Princeton, NJ 08544, USA

⁷ Institute of Astronomy, Faculty of Science, University of Tokyo, 2-21-1 Osawa, Mitaka, Tokyo 181-0015, Japan.

⁸ Harvard-Smithsonian Center for Astrophysics, 0 Garden St., Cambridge, MA 02138

$\vec{\alpha}(\theta_i)$ is the deflection field of the lens, $\vec{\beta}_s$ is the location of the source in the source plane and d_{ls}/d_s is the ratio of angular diameter distances from the lens to the source and from the observer to the source, respectively. Thus, predictions must be made for a wide range of background source distances unless the source redshift is known.

It should be appreciated that all the images of background galaxies lying within approximately twice the Einstein radii pertaining to their redshifts will have one or more lensed counter-images. Hence the usual identification of, at most, a few sets of multiple images per cluster, even in deep HST images, means the ‘‘eyeball’’ approach to finding counter-images can be far from exhaustive. We have had more success by using an iterative method, which we describe in §2.

Here we report the identification of three new examples of multiply imaged galaxies behind the cluster SDSS J1004+4112, and the measurement of spectroscopic redshifts for two of these. We use the multiply imaged galaxies and the five images of the QSO for a preliminary estimate of the cluster mass distribution. In a future paper (Ofek et al. 2005, in preparation), we will study more exhaustively the joint constraints that can be imposed on both the mass distribution and on the background cosmology. Throughout this paper we will assume cosmological parameters $H_0 = 70 \text{ km s}^{-1} \text{ Mpc}^{-1}$, $\Omega_m = 0.3$, and $\Omega_\Lambda = 0.7$.

2. IDENTIFICATION OF MULTIPLE IMAGES

We have examined the single-orbit ACS Wide Field Camera images of SDSS J1004+4112 taken in I (F814W) in 2004, April 28, and in V (F555W) in 2005, January 27, each with a total exposure time of 2025 s, obtained as part of the CASTLES program (GO-9744, Falco et al. 2001). Individual exposures in each band were processed and combined with the standard Space Telescope Science Institute pipeline. In addition to the final images in each band, we have produced a ‘‘true-color’’ image by assigning a blue color to the V count rate, red to the I count rate, and green to a linear interpolation of the V and I count-rates (see Fig. 1). Our goal is to identify multiple-image systems across as wide a range of redshifts as possible. In these data, we have identified three sets of multiply imaged galaxies, in addition to the known images of the lensed QSO.

The identification of multiply imaged galaxies is achieved in an iterative manner. We first construct a simplified mass model, as described in §4, initially based only on the images of the QSO. We de-lens the pixels belonging to any given faint object, using the lens model, onto a sequence of source planes of different distances, re-lens these pixels back to the image plane, and compare the model-predicted locations and morphology of the new counter-images with the data. As new images are identified, they are incorporated into a refined lens model, enhancing the prospects of finding further sets of multiply imaged galaxies.

The first set of lensed galaxy images to be identified in this way are labeled Galaxy A (A1-A5 in Figs. 1 and 2). They are observed as three arc-like images (A2, A3, A4) that lie well outside the Einstein ring traced by the QSO images. As seen in Fig. 1, the distance scale increases by a large factor between the redshift of the quasar and of Galaxy A. A counter-image of this galaxy is predicted

by the model and readily identified as A1, with an accurate reproduction of the internal morphology. A radial feature observed close to the central BCG (best seen in Fig. 2) could be a fifth counter-image of galaxy A. However, depending on the exact slope of the inner region of the mass profile, it could also be associated with other galaxies in the field. Deeper multi-color observations are required to confirm this possible association. This radial arc together with the fifth de-magnified image of the quasar will be helpful in constraining the inner mass distribution.

Two other sets of multiply imaged galaxies, Galaxies B and C, were identified using the best fit model based on galaxy A and the QSO. Each is identified as a close pair of images (see Figs. 1 and 2). Galaxy C has a different angular deflection scale, and therefore must lie at a higher redshift than galaxy B (see Table 1 for predictions). The model also predicts that galaxies B and C should both have faint, de-magnified images that are buried in the high surface brightness BCG and hence are undetectable in the available data.

3. SPECTROSCOPY

Multi-slit spectroscopy was carried out with LRIS on the Keck I 10 m telescope, on the nights of 2005, March 4 and 6, totaling 2.2 hrs of exposure time in dark conditions with $1''$ seeing. The D560 dichroic was used with the 400/3400 grism and 600/7500 grating at 6850 \AA , thus providing continuous wavelength coverage of $3500 \text{ \AA} \lesssim \lambda_{obs} \lesssim 7900 \text{ \AA}$. The FWHM spectral resolution and pixel scales were 6.8 \AA , 4.5 \AA and $0''.214 \text{ pixel}^{-1}$, $0''.135 \text{ pixel}^{-1}$ on the blue and red cameras, respectively.

Spectra were taken of the A2, A3 and A4 images of galaxy A, image B1 of galaxy B and image C1 of galaxy C.

Galaxy A – The one dimensional spectra extracted for A2, A3, and A4 (Fig. 3) clearly show that these are images of the same galaxy, although with some contamination of foreground galaxy light to A2 and A4. Several interstellar absorption lines were identified, from which we derive a redshift of $z = 3.332$ for Galaxy A.

Galaxy B – In galaxy image B1 (Fig. 1) we identified a single emission line at $\lambda_{obs}=4547 \text{ \AA}$, with an equivalent width of 80 \AA and intrinsic FWHM of 310 km s^{-1} . We interpret this line as Ly α redshifted to $z=2.74$, excluding the lower redshift alternative ([OII] at $z=0.22$, i.e., in front of the cluster) on the basis of the presence of multiple-images of this galaxy and the absence of H β and [OIII] in the red-arm spectrum. Since the instrumental resolution and the intrinsic width of the line are comparable, the Ly α profile appears relatively symmetric.

Galaxy C – We detected a weak continuum in C1, but no obvious spectral features. The redshift of Galaxy C therefore remains unconstrained spectroscopically.

In summary, we have measured the redshifts of two of the multiply imaged galaxies behind this cluster, the spectroscopic redshifts comparing favorably with the redshifts inferred from a lens model based only on the image positions and the quasar redshift.

4. GRAVITATIONAL LENS MODEL

The geometrical distribution of the lensed images indicates that the projected mass distribution is elliptical in

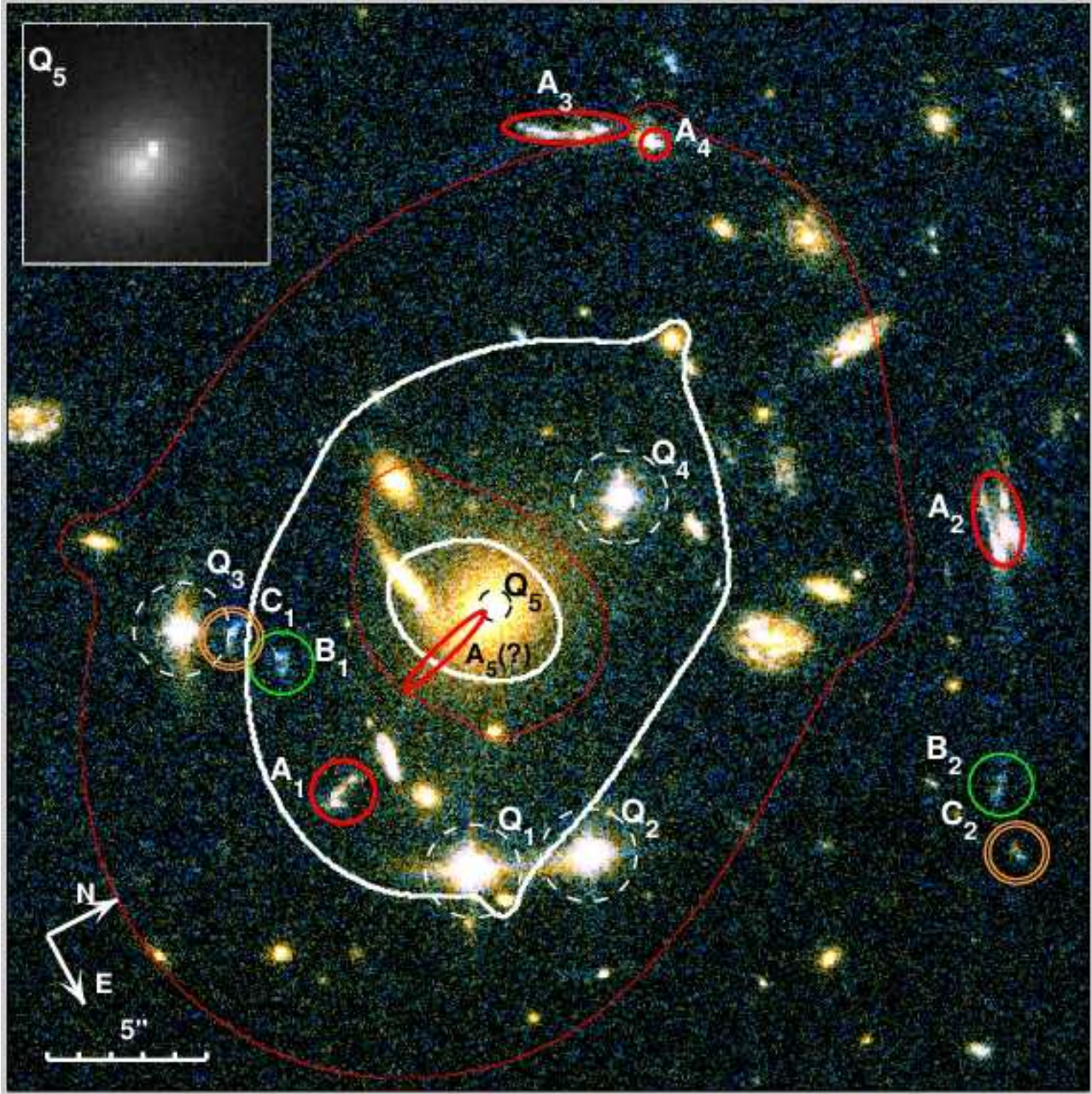


FIG. 1.— A color image of SDSS J1004+4112 produced from the ACS V - and I -band observations, with the images of the lensed galaxies and the QSO indicated. The inset shows the central region in I , where a faint fifth image of the lensed QSO is visible close to the center of the BCG. The fifth image is detected in both V and I , and has a $V-I$ color consistent with those of the other quasar images. Overlaid are the critical curves (radial and tangential), based on our model for the mass distribution, for the lensed QSO (white), and the corresponding critical curves for Galaxy A (red). Notice that the area enclosed by the Galaxy A tangential critical curve (essentially, the Einstein ring) is much larger ($\times 3.1$) than that of the QSO, due to the greater distance of Galaxy A ($z = 3.332$ vs. $z = 1.74$). The Vega-based I magnitudes of the galaxy images are: A1 23.4; A2 22.3; A3 22.4; A4 23.8; A5 26.6; B1 24.7; B2 25.0; C1 24.1; C2 24.8.

shape and lacks significant substructure. We have modeled the mass distribution with a softened power-law ellipsoid with surface density $\Sigma \propto \theta^{-\gamma}$ (Barkana 1998), plus contributions from red cluster members modeled as softened isothermal spheres and normalized according to their luminosity, and additional shear from a sub-group $15''$ to the northwest of the BCG, modeled as a softened power-law ellipsoid with $\gamma = 0.9$. We find that this simple model, with 15 free parameters (center of mass coordinates; slope, ellipticity, position angle, core

radius, normalizations of the cluster, galaxies and sub-group; and coordinates of the quasar and of galaxies A and B in the source plane), and the measured redshifts of galaxies A, B, and the quasar, are sufficient to fit the two-dimensional positions of 10 lensed images (Q1-Q5, A1-A3, B1, B2, i.e., 20 constraints) to a root-mean-square accuracy of $\sim 0''.1$ in the source plane.

The mass enclosed within a circular aperture including the images of galaxy A and corresponding to a radius ~ 110 kpc at the cluster redshift, is $6 \times 10^{13} M_{\odot}$. We

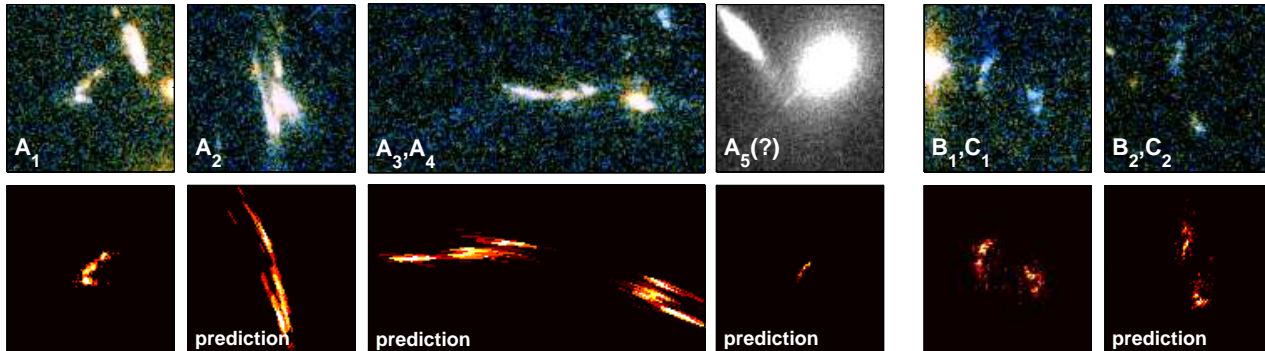


FIG. 2.— $V + I$ -based color renditions of the observed lensed sources (upper row) compared with the corresponding model-generated images in the lower row. The left-most image of each source is the template used to predict the structure of the other counter-images.

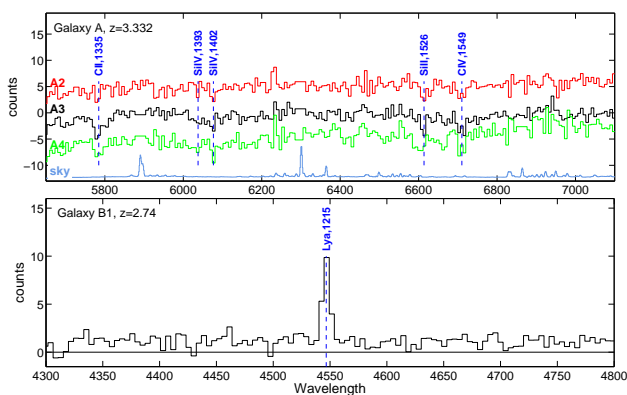


FIG. 3.— Top panel: Keck spectra (red arm) of images A2, A3 and A4 of Galaxy A, with identified spectral features for the derived redshift of $z = 3.332$. The A3 and A4 spectra have been vertically shifted for clarity. Sky subtraction residuals at 5892 Å, 6300 Å, and 6864 Å have been excised from the spectra – a sky spectrum, showing the main atmospheric emission lines, is shown for comparison. Slight differences in the spectra of the three galaxies are due to contamination of the spectra of A2 and A4 by the light of other galaxies, likely in the lensing cluster. Bottom panel: The blue-arm spectrum of image B1 of Galaxy B shows a strong emission line at 4547 Å, which we interpret as $\text{Ly}\alpha$ at $z = 2.74$. Spectra are binned to the spectral resolution.

find a mean projected slope of $\gamma \simeq 0.5$, considerably shallower than isothermal ($\gamma = 1$), but comparable to the projected surface density derived from CDM-based simulations of massive halos (e.g., NFW). This result is consistent with an earlier claim of $0.3 < \gamma < 0.5$ made by Williams & Saha (2004) using a nonparametric model based only on the quasar image positions. The ellipticity is relatively large, $e \simeq 0.55$ (suggesting the mass distribution may be more complicated than the current model; Edge et al. 2003) and the mass has a projected position angle of $\text{PA} \simeq 332^\circ$ (Fig. 1). The orientation of the cluster mass distribution is approximately aligned with the isophotes of the BCG and the position of the sub-group. In Figure 2, we illustrate how our model reproduces the morphologies of the lensed images of galaxies A, B, and C.

5. CONCLUSIONS AND FUTURE WORK

TABLE 1
SUMMARY OF MULTIPLY IMAGED SOURCE PROPERTIES

Source	No. of images	Relative deflection	predicted z	observed z
QSO	5	1.0	...	1.74
Galaxy A	5	1.32	3.57	3.332
Galaxy B	2	1.255	2.65	2.74
Galaxy C	2	1.215	2.94	...

We have identified three new multiply imaged galaxies in ACS images of the cluster lens SDSS J1004+4112, and have obtained redshifts for two of these systems. The relative deflections of the lensed quasar and the lensed galaxy images show a clear trend with redshift, increasing by $\simeq 30\%$ over the range $1.74 < z < 3.33$. The model-predicted deflection angles and the measured redshifts are found to be in good agreement with expectations from a model based on an elliptical, shallower-than-isothermal, mass distribution and the standard cosmological parameters.

In a future paper (Ofek et al. 2005, in preparation), we will investigate what regions of model parameter space can be excluded by the data, in terms of both the cluster mass distribution and the underlying cosmology, the latter dictating the ratios of angular diameter distances. The quality of the strong lensing constraints available for this cluster should help to break degeneracies between the parameterization of the cluster mass distribution and the cosmological world model. The high redshift of this cluster lens may also help to reduce uncertainties caused by large scale structure along the line-of-sight (Dalal et al. 2005). We will also investigate the possibility that the mass associated with some of the lensed galaxies (e.g., the quasar host galaxy) contributes to the lensing signal observed in more galaxies. If such a direct geometric measurement of cosmological parameters to a competitive accuracy is feasible, it will apply to a redshift range intermediate to those based on measurements of type-Ia supernovae and the cosmic microwave background. Furthermore, a lensing-based measurement will sample the $\Omega_m - \Omega_\Lambda$ parameter plane at an angle almost parallel to Ω_Λ and is therefore complementary to the two other methods.

Deeper, multi-wavelength imaging of SDSS J1004+4112 has been approved, using HST/ACS, HST/NICMOS, and the Spitzer Space Telescope. These data will likely reveal additional sets of multiply imaged galaxies, perhaps at even higher redshifts, as well as provide reasonably accurate photometric redshifts, beyond the reach of spectroscopy. Weak lensing measurements will also be feasible. Together with the strong lensing information, we will then attempt to tighten considerably the lens model and to estimate cosmological parameters based on this uniquely useful lens.

We thank Rennan Barkana for his help with the mod-

eling, and Phil Marshall for his assistance with the Keck observations. Some of the data presented herein were obtained at the W.M. Keck Observatory, which is operated as a scientific partnership among Caltech, the University of California and NASA. This work was supported by grant HST-GO-9744 (CSK and EEF) from the Space Telescope Science Institute which is operated by AURA, Inc., under NASA contract NAS5-26555; by a grant from the German Israeli Foundation for Research and Development (KS, EOO, and DM); and by a grant from the Israel Science Foundation (TJB). GPS acknowledges Caltech Optical Observatories for generously supporting his observations of high redshift galaxy cluster lenses.

REFERENCES

- Barkana, R. 1998, *ApJ*, 502, 531
 Benítez, N. 2000, *ApJ*, 536, 571.
 Broadhurst, T., et al. 2005a, *ApJ*, 621, 53
 Broadhurst, T., Takada, M., Umetsu, K., Kong, X., Arimoto, N., Chiba, M., & Futamase, T. 2005b, *ApJ*, 619, L143
 Bullock, J. S., Kolatt, T. S., Sigad, Y., Somerville, R. S., Kravtsov, A. V., Klypin, A. A., Primack, J. R., & Dekel, A. 2001, *MNRAS*, 321, 559
 Dalal, N., Hennawi, J. F., & Bode, P. 2005, *ApJ*, 622, 99
 Edge, A. C., Smith, G. P., Sand, D. J., Treu, T., Ebeling, H., Allen, S. W., & van Dokkum, P. G. 2003, *ApJ*, 599, L69
 Falco, E. E., et al. 2001, *ASP Conf. Ser. 237: Gravitational Lensing: Recent Progress and Future Go*, 237, 25
 Gavazzi, R., Fort, B., Mellier, Y., Pelló, R., & Dantel-Fort, M. 2003, *A&A*, 403, 11
 Inada, N., et al. 2003, *Nature*, 426, 810
 Inada, N. et al. 2005, *PASJ*, 57, L7
 Kneib, J. et al. 2003, *ApJ*, 598, 804
 Kochanek, C. S. 1991, *ApJ*, 382, 58
 Kochanek, C. S., & Dalal, N. 2004, *ApJ*, 610, 69
 Kochanek, C. S. et al. 2005, in preparation
 Moore, B., Ghigna, S., Governato, F., Lake, G., Quinn, T., Stadel, J., & Tozzi, P. 1999, *ApJ*, 524, L19
 Navarro, J. F., Frenk, C. S., & White, S. D. M. 1997, *ApJ*, 490, 493
 Ofek, E. O., et al 2005, in preparation
 Oguri, M., et al. 2004, *ApJ*, 605, 78
 Oguri, M., Takada, M., Umetsu, K., Broadhurst, T. J, *ApJ*, submitted (astro-ph/0505452)
 Sand, D. J., Treu, T., Smith, G. P., & Ellis, R. S. 2004, *ApJ*, 604, 88
 Smith, G. P., Kneib, J., Smail, I., Mazzotta, P., Ebeling, H., & Czoske, O. 2005, *MNRAS*, 359, 417
 Williams, L. L. R., & Saha, P. 2004, *AJ*, 128, 2631